



# Prediction of spatio-temporal land use/land cover dynamics in rapidly developing Varanasi district of Uttar Pradesh, India, using geospatial approach: a comparison of hybrid models

Varun Narayan Mishra<sup>1</sup> · Praveen Kumar Rai<sup>2</sup> · Rajendra Prasad<sup>1</sup> · Milap Punia<sup>3</sup> · Mărgărit-Mircea Nistor<sup>4</sup>

Received: 27 June 2017 / Accepted: 4 April 2018 / Published online: 22 May 2018  
© Società Italiana di Fotogrammetria e Topografia (SIFET) 2018

## Abstract

Land use/land cover changes (LULCC) are one of the foremost aspects of environmental changes caused by human-induced activities mainly in rapidly developing areas. This study endeavors to evaluate and compare three hybrid models: stochastic Markov chain (ST-MC), cellular automata-Markov chain (CA-MC), and multi-layer perceptron-Markov chain (MLP-MC) to predict future land use/land cover (LULC) scenario in Varanasi district. LULC information extracted for years 1988 and 2001 was first employed to predict LULC scenario for 2015 using three hybrid models. The predicted results were compared with the observed LULC information for the year 2015 to appraise the validity of models through kappa index statistics. The MLP-MC model yielded reliable and best results. Finally, based on this consequence, the prediction of future LULC scenarios for years 2030 and 2050 was performed. The findings of this study exhibited the constant but overall increase of built up area and a considerable reduction in agricultural land. The results also demonstrate the potentiality of MLP-MC hybrid model for better understanding of spatio-temporal dynamics and predicting future landscape scenario in Varanasi district of Uttar Pradesh, India.

**Keywords** LULCC · Stochastic · Cellular automata · Multi-layer perceptron · Markov chain · Prediction

## Introduction

Land use/land cover (LULC) is assumed to be an integral component of the terrestrial environmental system. LULC information plays a crucial role in investigating various environmental transform processes and climate change on local and global scales (Bonan 2008). The analysis and monitoring of LULC changes (LULCC) are vital for understanding com-

plex interactions between human activities and global environmental changes (Dickinson 1995; Zhu and Woodcock 2014). LULCC focuses mainly on spatio-temporal dynamics, and the human interferences largely influence the earth's environment by changing the dynamics of LULC (Thies et al. 2014). The alteration in LULC by human or natural activities come to rise various environmental concerns such as biodiversity loss, deforestation, global warming, and increase of natural disasters (Mas et al. 2004; Dwivedi et al. 2005). With growing population and increasing socioeconomic requirements, a pressure is created on LULC which leads to changes in it in a spontaneous and uncontrolled manner (Seto et al. 2002). Therefore, with increasing LULCC, mainly because of human activities, it is essential to identify such changes, appraisal of their trends, and effects on the environment for future planning and natural resource management (Prenzel 2004).

A significant amount of data is required for analyzing, monitoring, and quantifying the ongoing changes in LULC of an area. In recent years, the availability of remote sensing data from various satellite sensors has been of immense help in the field of LULCC studies (Miller et al. 1998; Zhu and

---

✉ Varun Narayan Mishra  
varun9686@gmail.com

<sup>1</sup> Department of Physics, Indian Institute of Technology (BHU), Varanasi, India

<sup>2</sup> Department of Geography, Institute of Science, Banaras Hindu University, Varanasi, India

<sup>3</sup> Centre for the Study of Regional Development, Jawaharlal Nehru University, New Delhi, India

<sup>4</sup> School of Civil and Environmental Engineering, Nanyang Technological University, Singapore, Singapore

Woodcock 2014; Mishra and Rai 2016). In several studies, the integration of remote sensing (RS) and geographical information systems (GISs) served as an efficient scheme for analyzing and detecting the spatial allocation of changes in LULC over large areas (Carlson and Azofeifa 1999; Kilic 2006). In recent years, the spatio-temporal modeling of LULC dynamics has drawn a lot of attention in solving the problems that occur due to the alteration and conversion of LULC (Lambin et al. 2001). The studies of modeling approaches for future scenarios depend on predictions, whereas the analyses and reviews of the past to the current depend on facts. However, the prediction of future situation is directly linked to the changes detected from the past to the current as well (Bhatta 2010).

The investigation of current situations and that of model applications both are spatial in nature; thus, the solutions also need a spatial approach. As a result, it is necessary to apply spatially explicit models to simulate and predict the changes in LULC with the purpose to appraise future scenarios. Consequently, accurate and timely information provided by RS technologies at regular interval can be applied efficiently to detect and analyze the past and current trends as well as to predict future trends of LULC (Dadhich and Hanaoka 2011; Mishra et al. 2014; Mishra and Rai 2016). The quality of predicted results is strongly affected by the accuracy of the investigation of past and current trends, the data quality, and the model applied for predictions (Mozumder and Tripathi 2014). Over the years, several spatially explicit models have been developed and used successfully by integrating RS and GIS to simulate and predict future LULC scenarios such as Markov chain (MC) model (Muller and Middleton 1994; Arsanjani et al. 2011; Fathizad et al. 2015), artificial neural network (ANN) model (Pijanowski et al. 2005; Mozumder and Tripathi 2014; Maithani 2015), cellular automata (CA) model (Clarke and Hoppen 1997; Mitsova et al. 2011), logistic regression (LR) model (Al-sharif and Pradhan 2014a; Kumar et al. 2014), GeoMod (Giriraj et al. 2008; Paudel and Yuan 2012), SLEUTH model (Jantz et al. 2003; Hua et al. 2014), and conversion of land use and its effects (CLUE) model (Veldkamp and Fresco 1996; Zhu et al. 2010). Every single model exhibits some advantages and disadvantages that have been described by Triantakou and Mountrakis (2012).

The MC analysis is an essential approach to model the landscape changes in describing and predicting the behavior of complex systems (Fortin et al. 2003). It is a convenient tool for modeling the LULC changes, when it is difficult to describe the modifications and processes in the landscapes. The MC produces a transition matrix by analyzing two qualitative LULC maps from different dates. A transition matrix is then employed as a basis to predict future scenario of a landscape. The MC model also computes the probability that a cell (pixel) will change from one LULC type (state) to another from the observed data within a specific period (Eastman 2006). The probability of changing from one state to another

is called a transition probability. The MC model theoretically assumes that the transition probability is spatially independent (Brown et al. 2000). However, the tendency of a changing cell in the future is not a simple function of its current state but is often influenced also by its neighboring cells. It does not consider the driving forces and processes that produced the observed patterns. As a consequence, the stand-alone MC model ignores the spatial distribution of changes (Araya and Cabral 2010). Therefore, additional steps are required to include both spatial and temporal information. The shortcomings of an individual model must be overcome by combining them to work as complementary to each other.

Therefore, in recent years, several hybrid models have been developed to improve dynamic process representation with the utility of MC model coupling with other models such as stochastic Markov chain (ST-MC) (Bozkaya et al. 2015), cellular automata-Markov chain (CA-MC) (Kamusoko et al. 2009; Al-sharif and Pradhan 2014b), and multi-layer perceptron-Markov chain (MLP-MC) (Thapa and Murayama 2012; Mishra and Rai 2016). The MC model is also integrated with other methods to improve the prediction of future scenarios of highly complex landscapes. For instance, Arsanjani et al. (2013) employed an integrated MC-LR model to generate accurate prediction maps for future land use changes for 2016 and 2026 with reasonable accuracy. Tang et al. (2007) used LULC information derived from Landsat data between 1979 and 2001 to predict future landscape distribution efficiently with the help of MC and genetic algorithm in Daqing City, China. Although the hybrid modeling approach provides better and improved understanding of modeling the changes in LULC (Guan et al. 2011), it is very challenging to find out a hybrid model that provides the best result because each study offers a unique conclusion, since the performance of LULCC modeling is different for different study areas because of varied environmental conditions and landscapes of that individual area (Arsanjani et al. 2011). Thus, instead of identifying a single model, the best result-providing model should be used for the study area. The comparison of models and prediction of the future LULC scenario using the best result-providing model is gaining more popularity in remote sensing community (Mas et al. 2014; Mozumder et al. 2016). Although a substantial number of research using MC-based models exists, comparison studies are still limited. The present study aims to evaluate the performance of three MC-based hybrid models: ST-MC, CA-MC, and MLP-MC to simulate and predict future LULC scenarios in Varanasi district of Uttar Pradesh, India. More specifically, the objectives of the present study are to (1) analyze the spatial and temporal patterns of LULCC in 1988–2001–2015; (2) simulate and predict scenarios of future LULC based on ST-MC, CA-MC, and MLP-MC; (3) determine the model that provides the better results in the study area; and (4) predict future scenarios of LULC for years 2030 and 2050 using the model providing best results.

Varanasi district of Uttar Pradesh, India, is one of the oldest living places in the world. It experienced rapid population growth and urban expansion in the last few decades. So, understanding the past changes in LULC and predicting the future scenarios are vital for proper future planning and sustainable management of the environment and natural resources. This information may also be precious for the recently launched smart city initiative by the Government of India. The outcomes of this study could be employed in other geographical locations of India and around the world.

## Study area

Varanasi district of Uttar Pradesh, India, is chosen for the present study. The area under investigation lies geographically between 25° 10' to 25° 37' N latitude and 82° 39' to 83° 10' E longitude, covering an area of approximately 1532.91 km<sup>2</sup>. It is located on the bank of holy river Ganga. It is famous for being a hotspot of heritage, education, and biodiversity for over many years. It lies physiographically in the middle Ganga plain and is very fertile and rich in agricultural productivity. Climatically, it experiences a humid subtropical climate with a significant difference between summer and winter temperatures. Figure 1 displays the geographical location of the study area as viewed on Landsat 8-OLI image.

The population expansion is one of the most intimidating issues in India. The growth of Varanasi district has been disorganized and largely unintended. The Varanasi district has a total population of 3,676,841 people with 1,921,857 males and 1,754,984 females. While in 2001, Varanasi had a population of 3,138,671 people with 1,649,187 males and 1,489,484 females (Census of India 2011). One of the most significant reasons for population growth in the Varanasi is the large-scale rural-to-urban relocation and rapid urbanization. In the year 2001, the population density was 2045 persons per km<sup>2</sup>, while in the year 2011, it increased up to 2395 persons per km<sup>2</sup>. The average literacy rate in the year 2001 was 66.12% and increased to 75.60% in the year 2011.

## Materials and methodology

Three phases are involved in this study to model and predict the spatio-temporal dynamics of LULC in Varanasi district of Uttar Pradesh, India. The first phase involved the collection of remote sensing images covering the study area and the preparation of LULC layers for different years. The second phase involved the analysis of LULCC. In the third and final phase, the factors affecting the changes in LULC were determined, and the LULC based on past changes and the factors was simulated and predicted. For the present study, remote sensing images of Landsat series satellites were employed to generate LULC layers

of Varanasi district of Uttar Pradesh, India. Remote sensing images of Landsat 5 Thematic Mapper (TM) acquired on 4 November 1988, Landsat 7 Enhanced Thematic Mapper Plus (ETM+) image acquired on 31 October 2001, and Landsat 8 Operational Land Imager (OLI) image acquired on 15 November 2015 were downloaded from the official website of the United States Geological Survey (USGS) (<http://glovis.usgs.gov>). The details of remote sensing images used in this study are represented in Table 1. In this study, digital elevation model (DEM) and road networks were used as auxiliary datasets. The SRTM DEM with 90 m spatial resolution was downloaded from <http://srtm.csi.cgiar.org/> and used to produce slope and aspect. The vector layer of road network and rail network were extracted from the toposheet and Google Earth images. All the subsequent pre-processing, interpretation, and LULC classification of multi-temporal remote sensing images were performed using ENVI (v 5.1) image processing software. Also, to model LULCCs using three hybrid models which are ST-MC, CA-MC, and MLP-MC, IDRISI Selva software has been employed as well as to predict the future LULC scenarios.

## Pre-processing of remote sensing images

The collected multi-temporal remote sensing images were atmospherically corrected using the QUick Atmospheric Correction (QUAC) module available in ENVI software and spatially referenced to a common UTM projection system (zone 44, north) with datum WGS 84. All the images were resampled to a pixel size of 30 m. An appropriate band combination is required to generate false-color composite (FCC) for all the images. The band combination of B4, B3, and B2 was used to generate FCCs for Landsat 5 TM and Landsat 7 ETM+ images. The band combination of B5, B4, and B3 was used to generate FCC for Landsat 8 OLI image. These FCCs were employed to create training samples (signatures) for LULC classification purpose. After the generation of training signatures, the separability analysis using a transformed divergence (TD) method was used to examine the quality of training signatures prior to image classification. Its values range from 0 to 2.0 and indicate how well the selected training signatures are statistically separated from each other. The separability analysis shows the range of values (from 1.75 to 2.0, where the average divergence is 1.96) for Landsat 5 TM data of 1988 (from 1.75 to 2.0, where the average divergence is 1.98), for Landsat 7 ETM+ data of 2001, and (from 1.76 to 2.0, where the average divergence is 1.99) for Landsat 8 OLI data of 2015, respectively.

## LULC classification and accuracy assessment

In this study, support vector machine (SVM), a machine learning technique, was used to produce LULC maps for years 1988, 2001, and 2015, respectively. SVM is a

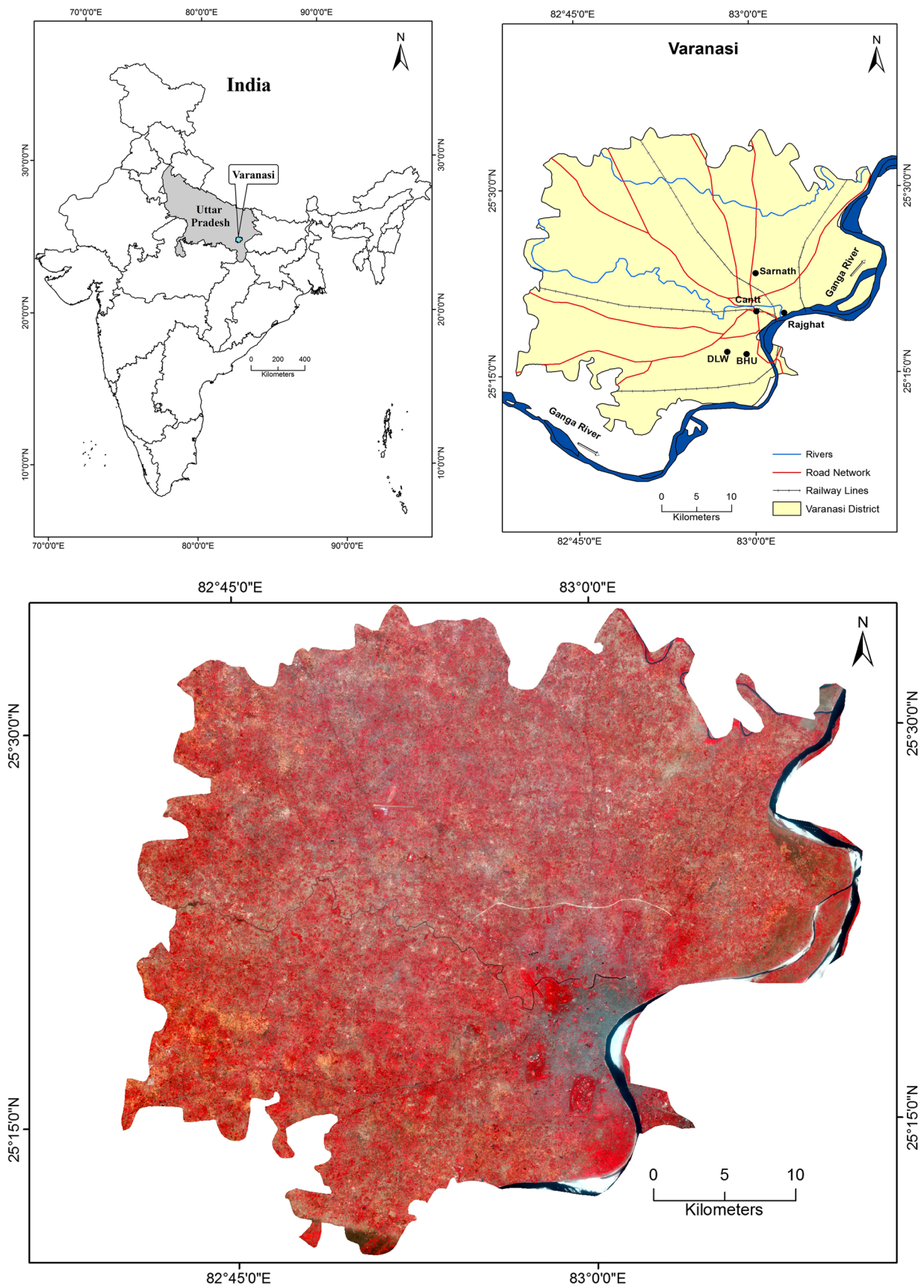


Fig. 1 Geographical location of the study area as viewed on Landsat 8-OLI image

**Table 1** Details of remote sensing images used in the study

Satellite sensor	Path/row	Date of acquisition	Spatial resolution (m)	Spectral bands ( $\mu\text{m}$ )
Landsat 5 TM	142/42	4 November 1988	30	B1 (blue), 0.45–0.52
			30	B2 (green), 0.52–0.60
	30		B3 (red), 0.63–0.69	
	30		B4 (NIR), 0.76–0.90	
	30		B5 (SWIR), 1.55–1.75	
	120		B6 (TIR), 10.40–12.50	
	30		B7 (MIR), 2.08–2.35	
Landsat 7 ETM+	142/42	31 October 2001	30	B1 (blue), 0.45–0.52
			30	B2 (green), 0.52–0.60
	30		B3 (red), 0.63–0.69	
	30		B4 (NIR), 0.77–0.90	
	30		B5 (SWIR-1), 1.55–1.75	
	60		B6 (TIR), 10.40–12.50	
	30		B7 (SWIR-2), 2.09–2.35	
	15		B8 (PAN), 0.52–0.90	
Landsat 8 OLI/TIRS	142/42	15 November 2015	30	B1 (coastal aerosol), 0.43–0.45
			30	B2 (blue), 0.45–0.51
	30		B3 (green), 0.53–0.59	
	30		B4 (red), 0.64–0.67	
	30		B5 (NIR), 0.85–0.88	
	30		B6 (SWIR-1), 1.57–1.65	
	30		B7 (SWIR-2), 2.11–2.29	
	15		B8 (PAN), 0.50–0.68	
	30		B9 (cirrus), 1.36–1.38	
	100		B10 (TIRS-1), 10.60–11.19	
	100		B11 (TIRS-1), 11.50–12.51	

supervised classification method based on statistical learning theory (Vapnik 1999). The radial basis function (RBF) kernel was used in the present study. This kernel requires less computational effort and can handle the nonlinear relationship between the training data and the entire dataset (Mishra et al. 2017). Two parameters of RBF kernel that is penalty parameter ( $C$ ) and gamma parameter ( $\gamma$ ) were set as default values. The pyramid parameter was set to be zero value to process the image at full resolution. Based on field information and landscape of the study area, all the images were classified into seven major LULC classes: agricultural land, dense vegetation, sparse vegetation, fallow land, built up, water bodies, and sand. The error matrix was calculated in order to examine the accuracy of classification results obtained for all the years. The accuracy assessment was carried in terms of the overall accuracy (OA), producer's accuracy (PA), user's accuracy (UA), and kappa coefficient (Kc) (Congalton and Green 1999). In addition, the F-score was computed for better evaluation of class-wise accuracies (Mishra et al. 2017)

## Analysis of LULCC

The analysis of LULCC illustrates and quantifies the differences between the images of the same area at different years. The LULC maps based on classification of Landsat TM/ETM+/OLI images of years 1988, 2001, and 2015, respectively, were used in order to quantify the LULCC within the study area. The changes occurred drastically affect the natural resources and environment. Thus, the recognition of changes and their causes would be helpful to determine probable future changes and various LULC scenarios. The analysis and detection of LULCC is based on the changes in LULC classes from time 1 to time 2 (Eastman 2009). In this study, cross-tabulation analysis was performed to quantify LULCC throughout 1988–2001 (period 1), 2001–2015 (period 2), and 1988–2015 (period 3), respectively. The gains and losses experienced by various LULC classes, contributions to net change in built up area, and analysis of the spatial trend of change for built up area and agricultural land were also investigated within the study area for period 1, period 2, and period 3.

## Prediction of future LULC scenarios

In the present study, three hybrid models, namely ST-MC, CA-MC, and MLP-MC, were employed to simulate and predict the LULC scenarios to a specified future date. A brief description of hybrid models is given as follows.

### ST-MC model

The functioning of the Markov model as a chain is known as Markov chain. It is used as a stochastic process in this model that integrates each single category as the state of a chain (Weng 2002). MC has been used broadly to model LULCC at large spatial scales (Muller and Middleton 1994) using discrete state spaces. The first model applied in this study is the ST-MC model because it combines both the stochastic processes and Markov chain analysis methods (Eastman 2009). The stochastic Markov chain model has been carried out using IDRISI Selva software. Before applying the stochastic module, Markov chain analysis was performed between LULC maps in 1988 and 2001 to predict LULC in 2015. This type of predictive LULCC model is appropriate when the past trend of a LULCC pattern is known (Basharin et al. 2004; Eastman 2009).

In Markovian processes, the future state of a system can be predicted not based on the past but rather the present. In the beginning, MC generates a transition probability matrix (Table 2), a transition area matrix (Table 3), and a set of Markovian conditional probability images (Fig. 2) by analyzing two LULC maps from two different dates (1988–2001) (Eastman 2009). After that, a single LULC map for future prediction is produced by aggregating all the Markovian conditional probability images. A stochastic choice decision model is used to perform this prediction. It generates a stochastic LULC map by assessing and combining the conditional probabilities in which each LULC can exist at each pixel location adjacent to a rectilinear random distribution of probabilities (Ahmed and Ahmed 2012).

### CA-MC model

In this study, CA-MC hybrid modeling approach was used to predict LULC scenarios for 2015, 2030, and 2050. It binds the concepts of CA, MC, multi-criteria evaluation (MCE), and multi-objective land allocation (MOLA) (Eastman et al. 1998) resultant into a distinct dynamic model. Cellular automaton can be defined as an agent or object having the capability to change its state from a rule that describes the new state to its previous state and those of its neighbors. The CA model is spatially dynamic in nature and commonly used for LULCC analysis and prediction (Adhikari and Southworth 2012). The CA system consists of four components: cells, states, neighborhoods, and rules (Barredo et al. 2003). A cell is the smallest spatial unit, and the cells immediately nearby to a certain cell are referred as the neighborhood. The next state of each cell is established by the

states of its neighborhood cells. The rules were used to describe the states of the cells for the future time step (Ahmed and Ahmed 2012). In the CA model, the transition rule of a cell from one LULC to another is based on the state of the neighborhood cells (Verbarg et al. 2004). The spatial component can be incorporated easily into CA, and simple rules are used by it to address dynamism with increased computational efficiency. The fundamental equation of the CA model can be given as

$$S(t, t + 1) = f(S(t), N) \quad (1)$$

where  $S$ ,  $t$ ,  $t + 1$ , and  $N$  are the states of discrete cellular, the time instant, the next future time instant, and the cellular field, respectively, and  $f$  represents the transition rule of cellular states in local space, respectively.

The MC is a potential model for predicting land change demand when it is ambiguous to describe the changes and processes in LULC. It defines the future state of the environment solely according to the previous state. The MC model is a stochastic process that explains how likely one state is to transform into another and use it as the base to project changes in the future. The critical attribute of the MC is the development of transition probability matrix of changes in LULC from time to time, which can be used to predict the future status through the analysis of past situations. Although it is convenient to model the changes and determine the future trends using the MC approach, MC cannot be used solely for providing the information about the spatial allocation of these phenomena. Thus, the CA is utilized to describe the spatial components. In an integrated CA-MC model, CA deals with spatial dynamics using local transition rules while MC illustrates the temporal dynamics between LULC classes using transition probabilities (Eastman 2006).

In this study, cellular automata analysis was carried out by the CA\_Markov module in IDRIS Selva software. It uses a transition area matrix, a transition probability matrix, and a set of transition probability maps showing the probability of each pixel to a specific LULC class. A transition probability matrix based on the cross-tabulation of two LULC maps of different years is produced and determines the probability of changing of a pixel from a LULC class into another class during that time epoch. Also, a transition area matrix includes the number of pixels that are probable to change to a LULC class from another class during the time epoch. Thus, a contiguity filter of  $5 \times 5$  kernel size accounting the neighborhood pixels is applied to predict LULC from a time epoch to a later time epoch.

**Generation of suitability maps for LULC classes** In CA-MC, it is required to determine the transition potentials to model the changes in LULC. The suitability maps are used as transition potential (Olmedo et al. 2013). The pixels that will change as per the highest suitability of each LULC class are determined by the suitability maps. If the suitability of a pixel is higher, the likelihood of the neighboring pixels to change into that particular

**Table 2** Markov transition probabilities of change among LULC (1988–2001) for 2015

LULC class	Agricultural land	Dense vegetation	Sparse vegetation	Fallow land	Built up	Water bodies	Sand
Agricultural land	0.1722	0.0811	0.3304	0.1471	0.2632	0.0057	0.0003
Dense vegetation	0.3185	0.1403	0.4581	0.0416	0.0318	0.0089	0.0008
Sparse vegetation	0.4396	0.1110	0.3147	0.0997	0.0278	0.0071	0.0001
Fallow land	0.4230	0.0845	0.3413	0.1218	0.0084	0.0148	0.0062
Built up	0.0365	0.0296	0.0389	0.0372	0.8293	0.0194	0.0091
Water bodies	0.0785	0.0520	0.1695	0.0857	0.0211	0.4669	0.1263
Sand	0.0591	0.0010	0.0618	0.2234	0.0010	0.2595	0.3945

class is higher. But, it is complicated to prepare suitability maps for LULC classes in terms of data and information availability. Also, the incorporation of all types of factors or constraints that exist in the study area is not possible. Therefore, a fuzzy factor standardization procedure is assumed to be a simple assumption in this case. In suitability images, values 0 and 255 are unsuitable and highly suitable, respectively (Eastman 2009). Therefore, in this case, a simple linear distance decay function is appropriate. In this study, multi-criteria analysis based on a fuzzy linear function was utilized to generate suitability images of seven for each LULC class and is shown in Fig. 3. The criteria of suitability maps were established by the observable pattern of past land transformation circumstances. The fuzzy linear function is a decision-making process used to decide weights of selected criteria and constraints. Eventually, the prediction of LULC map of 2015 is carried out by utilizing the Markov transition area matrix, all the suitability images, the  $5 \times 5$  CA contiguity filter, and the LULC of 2001 as a base map.

### MLP-MC model

The world's ANN is synonymic to the human brain (Mas and Flores 2008). ANN has advantages over statistical methods because it does not assume probabilistic models of data. It can understand complex patterns present in the database and model complex nonlinear relationships (Ji 2000; Atkinson and Tatnall 1997). Although many neural network models have been developed, the multi-layer perceptron neural network (MLPNN) is broadly used in different applications (Hu and Weng 2009;

Mozumder and Tripathi 2014; Mishra et al. 2014). The MLPNN includes an input layer, many hidden layers, and an output layer. One of the main advantages of MLPNN is its capability to model several or even all the transitions at one time. It is trained by supervised backpropagation (BP) algorithm and provides the best generalization potential for transition of each LULC and simulation (Maithani 2015; Mishra et al. 2014). It also combines the variables affecting the LULC transitions (Mishra and Rai 2016). The MC quantifies changes in LULC and determines transition probability areas to predict probable LULCC in the future (Dadhich and Hanaoka 2011). In MLP-MC hybrid approach, the transitions are modeled using an MLPNN. The integration of MLP and MC takes the advantages of both the models. A prediction model of future LULC scenario was designed within the MLP-MC structure available in the land change modeler (LCM) module embedded in IDRISI Selva software. The LCM is a suite of tools for the rapid assessment of changes, evaluation of gains and losses, net change, persistence and identification of transitions between LULC classes both in map, and statistical and graphical appearance (Eastman 2006). It facilitates users to model and predict the future landscape scenario by incorporating user-defined drivers of changes (Eastman 2009). The LCM has more mapping facilities: the map transition and spatial trend of change are also utilized for further representation of the change detection and analysis.

### Selection of transitions and variables for model development

All the minor and major transitions occurred in LULC between two dates. With the aim of this study, only some of the major

**Table 3** A transition area matrix (1988–2001)

LULC class	Agricultural land	Dense vegetation	Sparse vegetation	Fallow land	Built up	Water bodies	Sand
Agricultural land	1,060,174	260,787	1,091,732	372,931	37,290	20,767	810
Dense vegetation	172,386	75,721	247,299	22,441	17,138	4817	0
Sparse vegetation	978,102	247,028	700,018	221,868	61,844	15,746	172
Fallow land	347,646	69,466	280,430	100,088	6918	12,198	5040
Built up	17,446	4947	34,768	7053	98,705	3079	1260
Water bodies	12,635	8380	27,295	13,804	3394	75,175	20,322
Sand	2694	46	2821	10,190	46	11,824	17,994

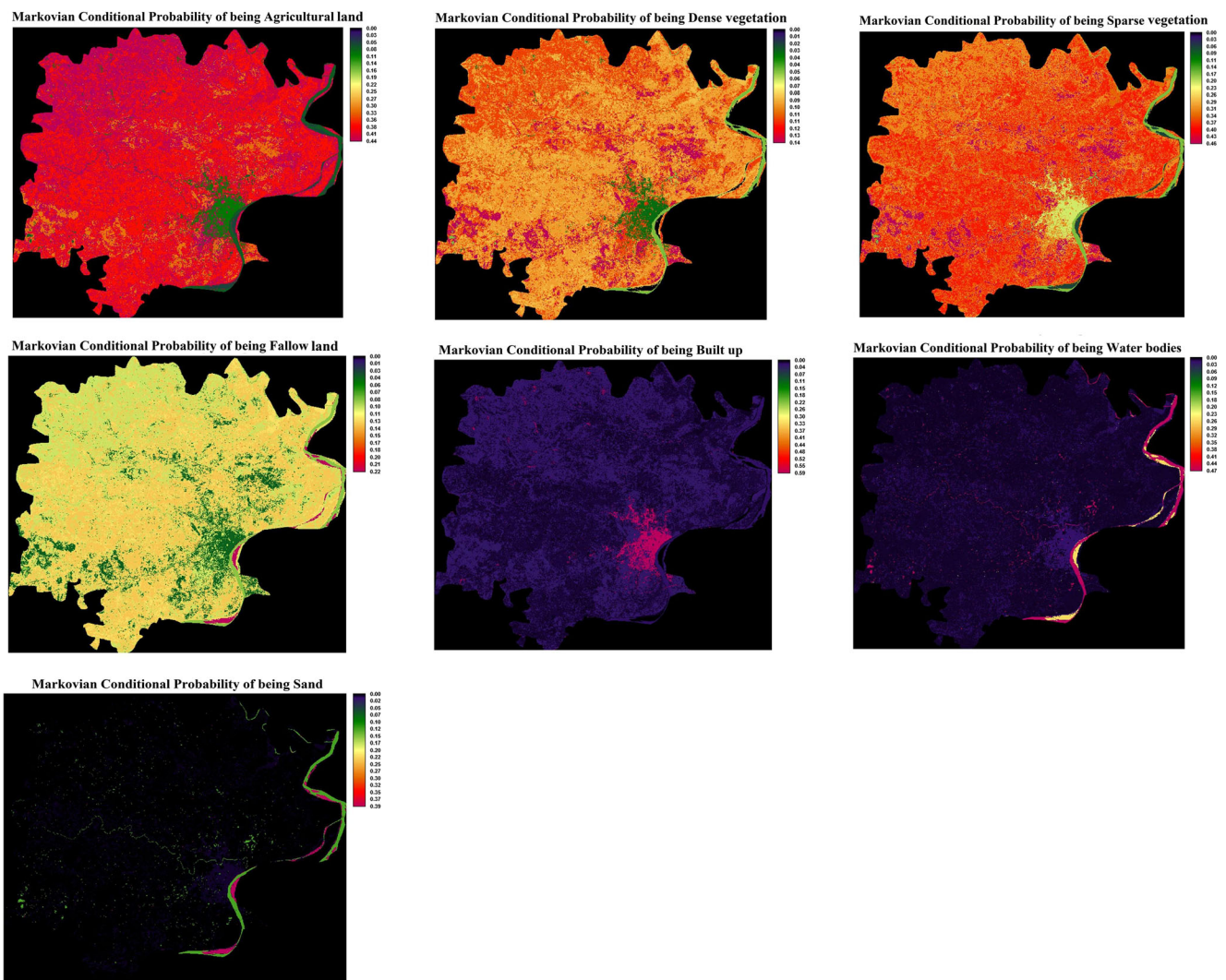


**Fig. 2** Markovian conditional probability images

transitions that occurred among LULC classes were considered. Only the significant transitions were included in transition submodel to improve the performance of MLPNN and get better results (Eastman 2006). The possible factors driving LULCC in Varanasi district of Uttar Pradesh, India, are characterized by nine major transitions: agricultural land to fallow land, agricultural land to built up, fallow land to agricultural land, fallow land to built up, dense vegetation to built up, dense vegetation to sparse vegetation, sparse vegetation to built up, sparse vegetation to fallow land, and water bodies to sand.

The transition potential was determined by developing submodels in the MLP-MC approach. All the observed LULC transitions were collected into a set of submodel. Each submodel is added by significant variables as either static or dynamic (Eastman 2006). A total of six environmental variables are considered in this study. Elevation, slope, and aspect were considered as the static variables, while the distance from major roads, distance from rail network, and distance from built up area were regarded as the dynamic

variables. An empirical likelihood to change map which is a qualitative variable was also produced besides these six quantitative variables. For producing this, a map showing changes from all LULC classes to built-up area was prepared. An empirical likelihood transformation is an effectual way of including categorical variables into the analysis. It is produced from the frequency of each LULC class that occurred within the areas of transition (Eastman 2009). All the seven explanatory variables used for the transition potential modeling are shown in Fig. 4. Now, the potential explanatory power of these variables was tested using Cramer's V statistics. It is recommended that the variables having a Cramer's V value of about 0.15 or higher are regarded as useful while those of about 0.4 or above are good (Eastman 2009). After getting acceptable Cramer's V values for all the driving variables, now, the MLPNN model was run using BP algorithm.

The prediction results are also influenced by constraints and factors. The expansion of built up area is restricted by some criteria known as constraints. In the present study, major roads



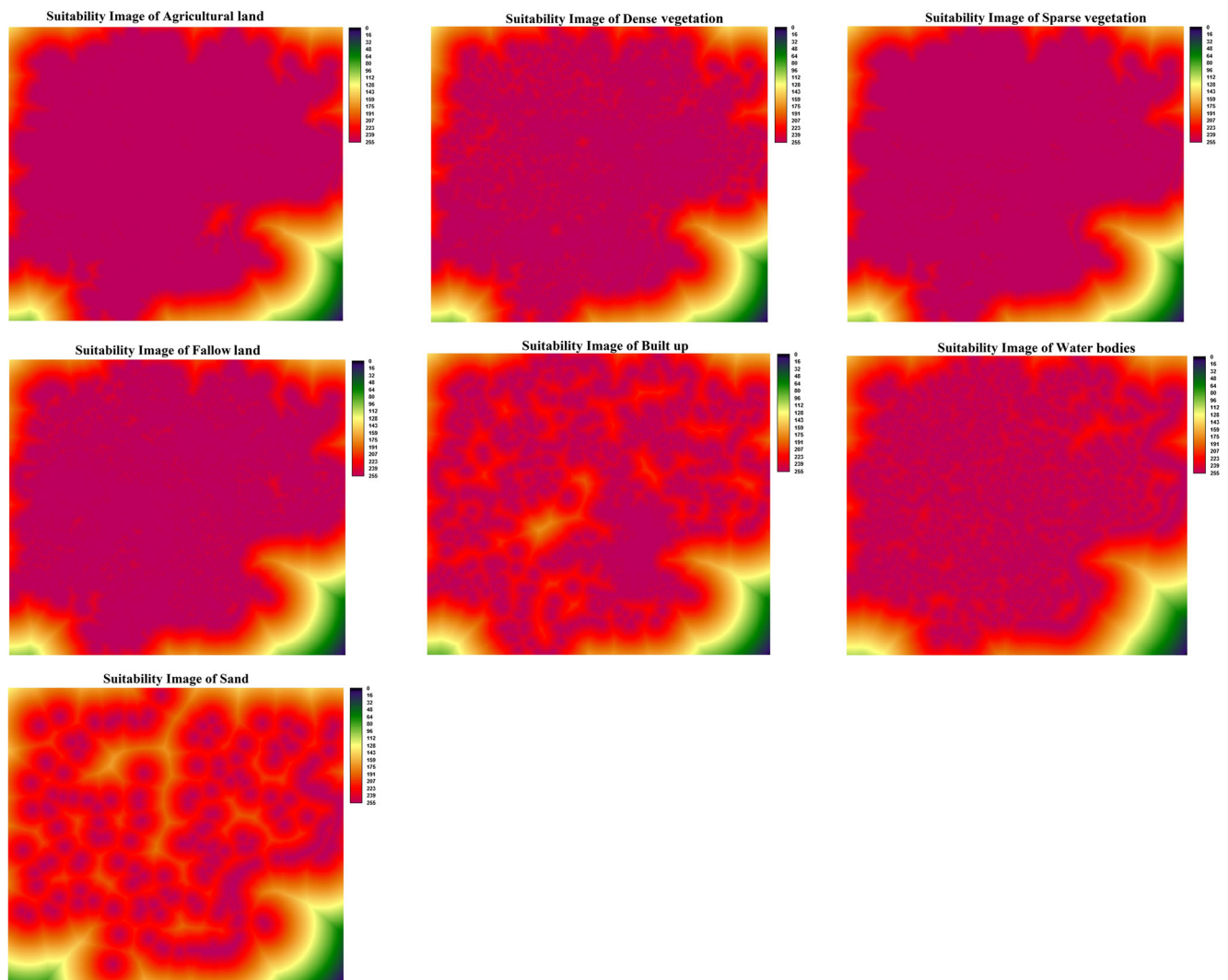


**Fig. 3** Suitability images of each LULC class

and rail network were considered as the constraints and are shown in Fig. 5. The reason behind choosing the distance from major roads as a factor is that most of the construction and developmental activities are supposed to take place along the roads. Two model variables such as major LULC transitions and driving factors were previously defined. On the basis of this information, transition potential maps were created to visualize the suitability of LULC classes for the future LULC scenario.

**Transition potential modeling** The transition potential maps were produced using seven variables as input, LULC transitions to be modeled, and MLPNN integrated into LCM. The MLP first creates a random sample of cells that transitioned among LULC classes during the required time and starts the automatic training process. It keeps 50% of the samples for training and the remaining 50% for testing the performance. In this study, the minimum number of cells that transitioned during 1988 to 2001 was chosen as 7959 to run MLP with 10,000 iterations. After running MLP, it was completed with an accuracy rate of 87.56%

which is a measure of calibration. It is recommended that accuracy rate more than 80% is acceptable (Eastman 2009). After the successful execution of MLP training, transition potential modeling is applied to generate transition potential maps. The amount of changes using the previous and later LULC maps was determined by the MC process and used to estimate the changes during the prediction process. The MC analysis also calculates the transition probability matrix of changing from one LULC class to another using past and current probabilities. Finally, the generated transition potential maps were further applied to predict LULC scenarios for future dates. By using this information, transition potential maps were produced to visualize the suitability of LULC classes for future scenarios.

### Validation of predicted results

If the evaluation of prediction provides convincing results, the hybrid models can be applied further for the prediction of future LULC scenarios (Moghadam and Helbich 2013). In

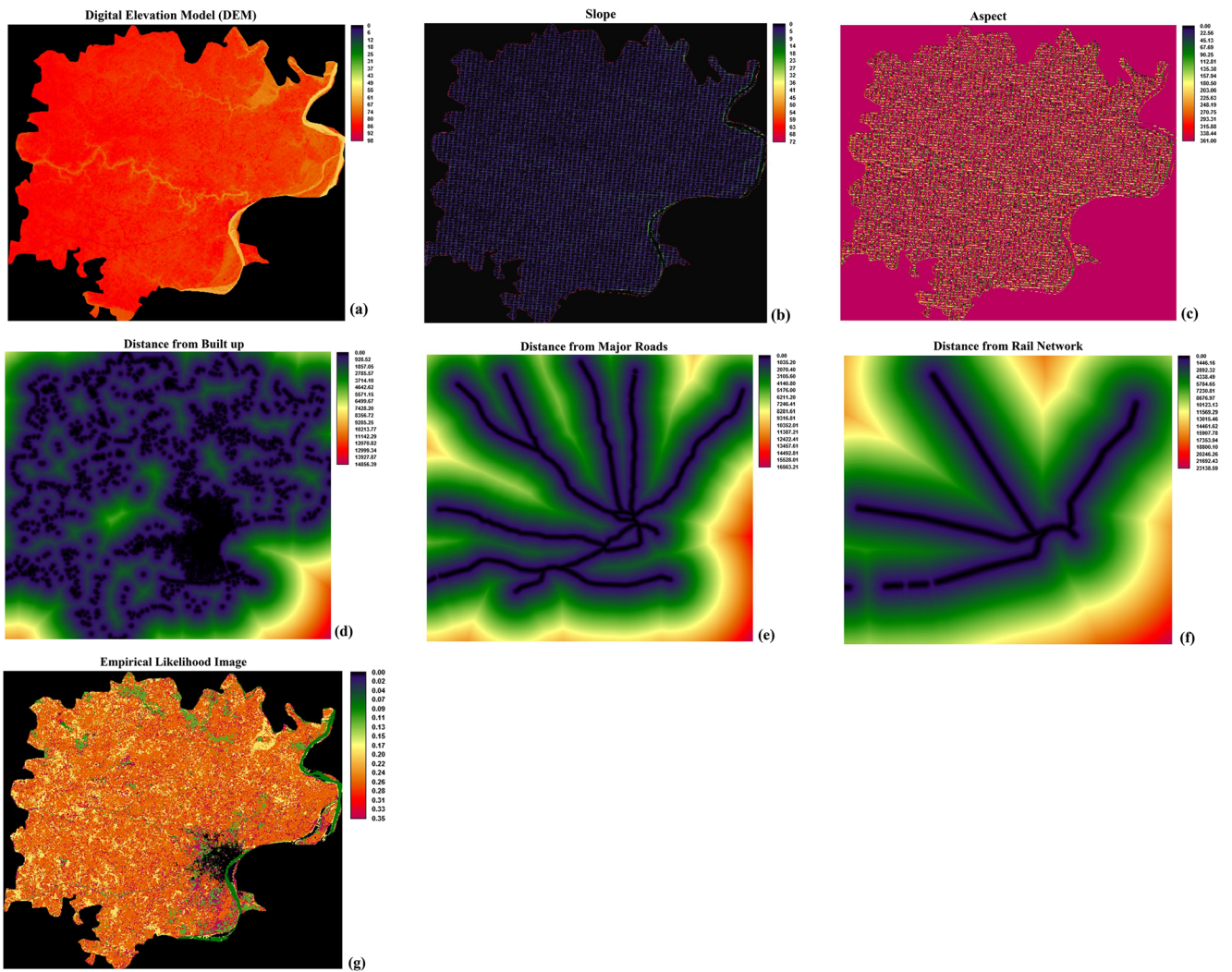


**Fig. 4** Explanatory variables. **a** DEM. **b** Slope. **c** Aspect. **d** Distance from built up. **e** Distance from major roads. **f** Distance from rail network. **g** Empirical likelihood image

general, the model validation is carried out by comparing the predicted and observed results. For this purpose, the LULC for the year 2015 was first predicted by ST-MC, CA-MC, and

MLP-MC hybrid models based on LULC information from 1988 and 2001. The predicted results were then compared with the actual LULC information observed by remote

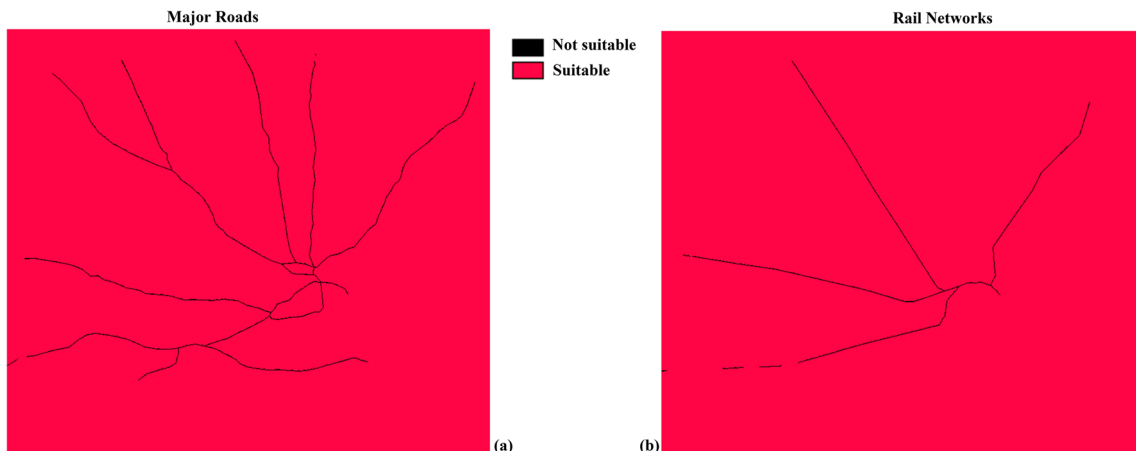


**Fig. 5** Constraints used in this study. **a** Major roads. **b** Rail network

**Table 4** Area distribution of LULC of years 1988, 2001, and 2015

LULC class	Year					
	1988		2001		2015	
	Area (km <sup>2</sup> )	Area (%)	Area (km <sup>2</sup> )	Area (%)	Area (km <sup>2</sup> )	Area (%)
Agricultural land	965.86	63.01	873.78	57.00	909.83	59.35
Dense vegetation	86.64	5.65	121.54	7.93	65.94	4.30
Sparse vegetation	178.82	11.67	263.66	17.20	204.74	13.36
Fallow land	225.68	14.72	182.68	11.92	193.86	12.65
Built up	26.71	1.74	45.63	2.98	123.48	8.06
Water bodies	39.68	2.59	35.26	2.30	23.48	1.53
Sand	9.51	0.62	10.36	0.68	11.59	0.76
Total	1532.91	100	1532.91	100	1532.91	100

sensing image of 2015 with the help of kappa index statistics to test the validity regarding quantity and location (Kamusoko

et al. 2009; Wang et al. 2012). The kappa index statistics includes the kappa for no information ( $K_{no}$ ), kappa for grid

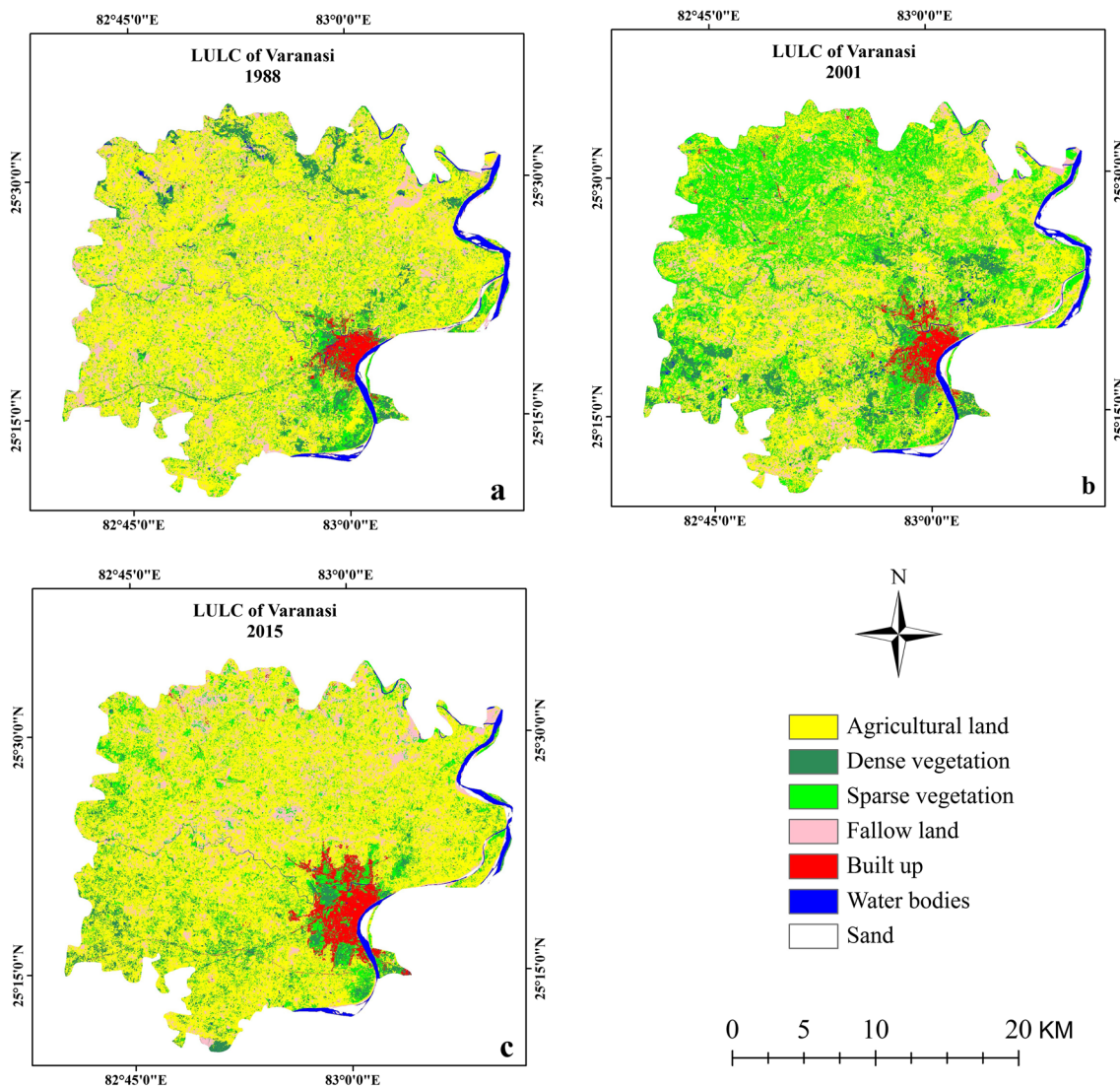


**Fig. 6** Classified LULC maps of Varanasi of years 1988 (a), 2001 (b), and 2015 (c)

**Table 5** Accuracy assessment of classified LULC maps of years 1988, 2001, and 2015

LULC class	Year								
	1988			2001			2015		
	PA (%)	UA (%)	F-score (%)	PA (%)	UA (%)	F-score (%)	PA (%)	UA (%)	F-score (%)
Agricultural land	83.78	84.55	84.55	87.27	88.07	87.67	88.29	89.91	89.09
Dense vegetation	89.36	91.30	90.32	90.53	92.47	91.49	89.32	90.20	89.76
Sparse vegetation	86.61	87.39	87.00	87.16	87.16	87.16	88.39	90.00	89.19
Fallow land	84.91	79.65	82.19	85.98	81.42	83.64	85.71	84.96	85.33
Built up	88.29	90.74	89.50	89.09	91.59	90.32	88.99	88.99	88.99
Water bodies	88.35	94.79	91.46	91.58	96.67	94.05	92.39	94.44	93.41
Sand	87.76	81.90	84.73	90.83	86.84	88.79	92.71	87.25	89.90
OA (%)	86.94			88.84			89.25		
Kc	0.8475			0.8697			0.8745		

cell-level location ( $K_{\text{location}}$ ), kappa for stratum-level location ( $K_{\text{location strata}}$ ), and kappa standard ( $K_{\text{standard}}$ ) which is similar to kappa (Pontius 2000).

## Results and discussion

To understand spatio-temporal dynamics of LULC, the results were divided into four components: (1) composition of the LULC maps and an accuracy assessment for the years 1988, 2001, and 2015; (2) change analysis of the periods 1988–2001 (period 1), 2001–2015 (period 2), and 1988–2015 (period 3); (3) prediction for the year 2015 by the ST-MC, CA-MC, and MLP-MC models, comparison of the prediction results with the observed LULC map of 2015, and identification of the model that provides the highest accuracy in the study area; and (4) prediction of future scenarios of LULCC for the years 2030 and 2050 using the best result-providing model that produced the best results in the prediction of year 2015.

## LULC maps and accuracy assessment

In this study, an SVM classifier was used to derive LULC maps for years 1988, 2001, and 2015. The distribution of different LULCs quantitatively and spatially for three different years (1988, 2001, and 2015) is shown in Table 4 and Fig. 6, respectively. After the classification of multi-temporal remote sensing images, the obtained OA is the indicator of the reliability and usability of classified results. The outcome of this procedure signifies whether the LULCC has been correctly identified and extracted. The PA, UA, and F-score were achieved by an error matrix approach, and the OA and Kc are listed in Table 5. The OA values of LULC maps for years 1988, 2001, and 2015 are 86.94, 88.84, and 89.25%, respectively. The Kc values for years 1988, 2001, and 2015 are 0.8475, 0.8697, and 0.8745, respectively. In this study, the accuracy assessment of the classified products of the respective years confirmed that the results are acceptable for many applications.

**Table 6** Amount of changes in LULC during period 1, period 2, and period 3

LULC class	Amount of changes					
	Period					
	1988–2001		2001–2015		1988–2015	
	Area (km <sup>2</sup> )	Area (%)	Area (km <sup>2</sup> )	Area (%)	Area (km <sup>2</sup> )	Area (%)
Agricultural land	–92.08	–6.01	36.05	2.35	–56.04	–3.66
Dense vegetation	34.90	2.28	–55.59	–3.63	–20.70	–1.35
Sparse vegetation	84.83	5.53	–58.92	–3.84	25.91	1.69
Fallow land	–43.00	–2.81	11.18	0.73	–31.82	–2.08
Built up	18.93	1.23	77.85	5.08	96.78	6.31
Water bodies	–4.43	–0.29	–11.78	–0.77	–16.21	–1.06
Sand	0.85	0.06	1.22	0.08	2.07	0.14

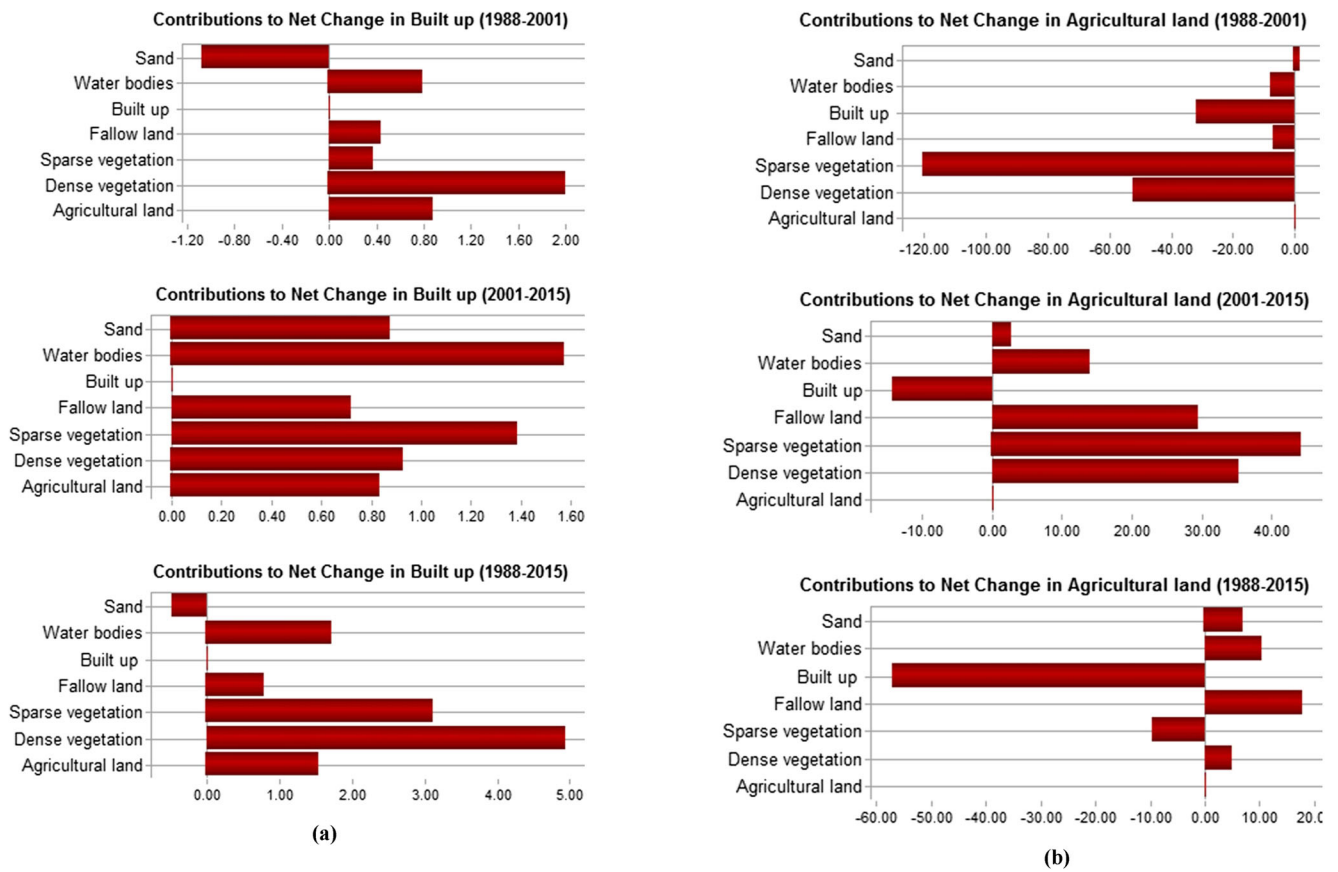


Fig. 7 Contributions to net change in a built up and b agricultural land (in % change)

**Analysis of LULCC**

The study area experienced drastic changes in LULC and was analyzed during period 1, period 2, and period 3. There are significant changes that occurred in all LULC classes particularly in agricultural land, fallow land, built-up area, and water bodies over the year (1988–2015).

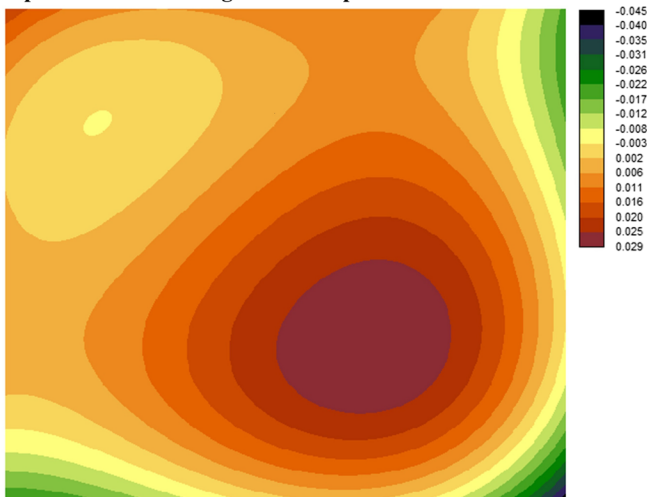
The agricultural land in 1988 covered an area of 965.86 km<sup>2</sup> (63.01%), and it decreased to 873.78 km<sup>2</sup> (57.00%) and 909.83 km<sup>2</sup> (59.35%) in 2001 and 2015, respectively. During period 1, the agricultural land reduced by 6.01%, while during period 2, it raised by 2.35%, and during period 3, it again reduced by 3.66%. The area covered by dense vegetation in 1988 was 86.64 km<sup>2</sup> (5.65%), and it increased to 121.54 km<sup>2</sup> (7.93%) in 2001 while it decreased in 2015 to 65.94 km<sup>2</sup> (4.30%). During period 1, the dense vegetation raised by 2.28%, while during period 2, it decreased by 3.63% and again decreased by 1.35% during period 3. The sparse vegetation covered an area of 178.82 km<sup>2</sup> (11.67%) in 1988, and it increased to 263.66 km<sup>2</sup> (17.20%) and 204.74 km<sup>2</sup> (13.36%) in 2001 and 2015, respectively. During period 1, the sparse vegetation raised by 5.53%, while during period 2, it decreased by 3.84% and again increased by 1.69% during period 3. The fallow land occupied an area of 225.68 km<sup>2</sup> (14.72%) in 1988, and it reduced to 182.68 km<sup>2</sup>

(11.92%) and 193.86 (12.65%) in 2001 and 2015, respectively. During period 1, the fallow land reduced by 2.81%, while during period 2, it slightly increased by 0.73% and again reduced by 2.08% during period 3. It was examined that in 1988, built up area covered an area of 26.71 km<sup>2</sup> (1.74%) and it increased to 45.63 km<sup>2</sup> (2.98%) in 2001 and 123.48 km<sup>2</sup> (8.06%) in 2015, respectively. The built up area raised by 1.23, 5.08, and 6.31% during period 1, period 2, and

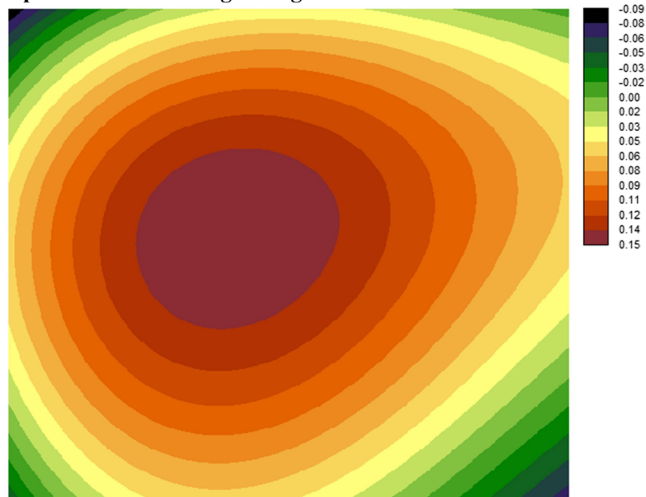
**Table 7** Annual rate of change during period 1, period 2, and period 3

LULC class	Annual rate of change (%)		
	Period		
	1988–2001	2001–2015	1988–2015
Agricultural land	−0.77	0.29	−0.22
Dense vegetation	2.60	−4.37	−1.01
Sparse vegetation	2.99	−1.81	0.50
Fallow land	−1.63	0.42	−0.56
Built up	4.12	7.11	5.67
Water bodies	−0.91	−2.90	−1.94
Sand	0.66	0.80	0.73

Spatial trend of change in Built up between 1988-2001

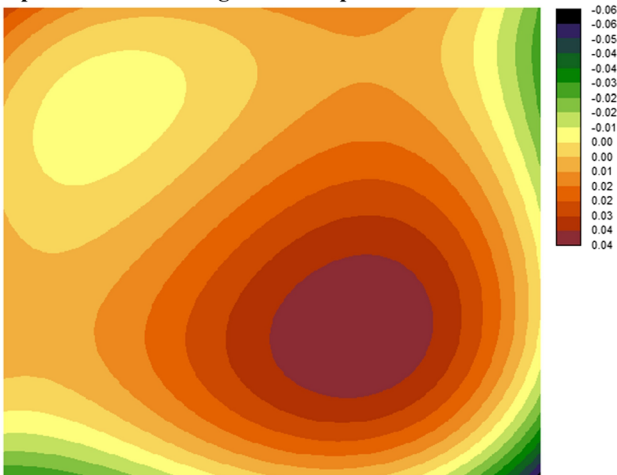


Spatial trend of change in Agricultural land between 1988-2001

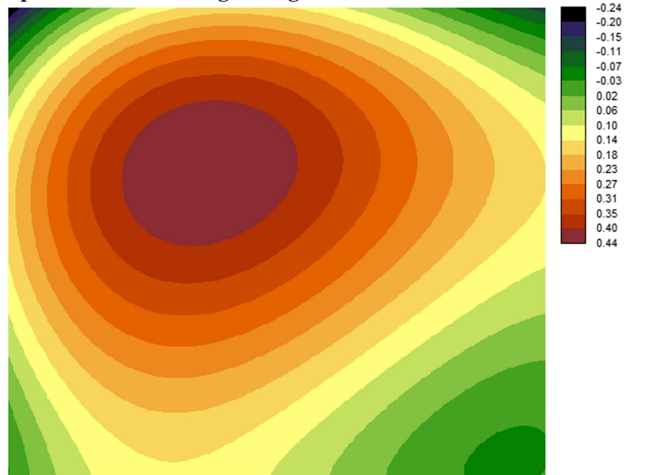


(a)

Spatial trend of change in Built up between 2001-2015

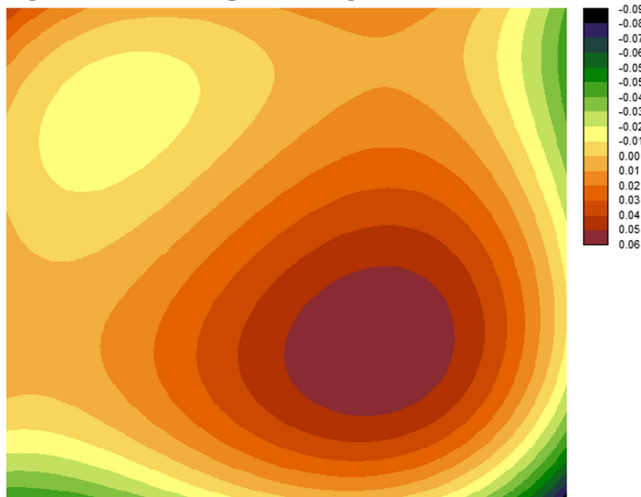


Spatial trend of change in Agricultural land between 2001-2015

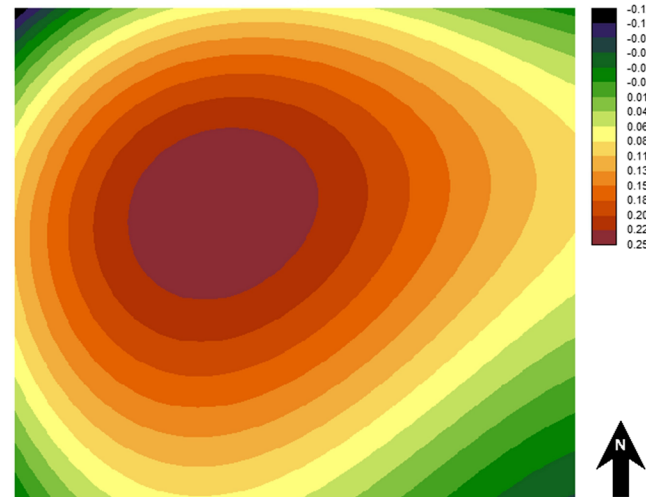


(b)

Spatial trend of change in Built up between 1988-2015



Spatial trend of change in Agricultural land between 1988-2015



(c)

Fig. 8 Spatial trend of change in built up and agricultural land during a period 1, b period 2, and c period 3

period 3, respectively. The continuous decrease in water bodies is observed by 0.29, 0.77, and 1.06% during period 1, period 2, and period 3, respectively. Sand is increased slightly by 0.06, 0.08, and 0.14% during all the periods.

An enormous change of 6.31% in built up area is observed between 1988 and 2015. Following this, there is a loss of 3.66, 2.08, and 1.35% in agricultural land, fallow land, and dense vegetation, respectively. The loss of agricultural land, fallow land, and dense vegetation contributed to an increase in the built up area between 1988 and 2015. This could be due to population growth linked with the requirement of land and urban supplies. The amount of changes in LULC during period 1, period 2, and period 3 is given in Table 6. The changing pattern between LULC classes and contributions to net change in built-up area and agricultural land during period 1, period 2, and period 3 is demonstrated in Fig. 7a, b.

During period 3, the rate of loss of water bodies is found maximum with  $-1.94\%$  followed by dense vegetation with  $-1.01\%$ , fallow land with  $-0.56\%$ , and agricultural land with  $-0.22\%$ . The highest positive rate of change is found for built up area with  $5.67\%$  followed by sand with  $0.73\%$  and sparse vegetation with  $0.50\%$ . It signifies that built-up areas have the highest positive rate of change while the water bodies had the highest negative rate of change during period 3. The water bodies and dense vegetation with the higher negative rate of change may be a major concern in the study area. The complete information about the rate of change for each LULC class during period 1, period 2, and period 3 is shown in Table 7.

### Analysis of spatial trend of change

The spatial trend of change analysis is an effectual approach to visualize and provide the generalized patterns of changes by using two observed LULC maps. The spatial trend of transitions from all LULC classes to built up area and agricultural land during period 1, period 2, and period 3, respectively, is shown in Fig. 8a–c. The spatial trend of change maps is created with the help of third-order polynomial parameter. The

numeric values in legends do not have any meaning (Eastman 2012). The lower or higher values exhibit less or more changes. The spatial trend of change maps shows that the agricultural land is shifted towards the eastern and southern directions during all the periods. It is also observed that the transition of built up area is more concentrated in the middle of the study area and expanding towards the northern and western directions during all the periods relative to other directions.

### ST-MC model-based prediction

The prediction of future LULCC scenario was conducted using a spatial transition ST-MC model. Firstly, MC produces a transition probability matrix, a transition area matrix, and a set of Markovian conditional probability images by analyzing LULC maps of two different dates (1988 and 2001) (Eastman 2009).

The transition probability matrix illustrates the probability that each LULC class will change to other classes in 2015. The Markovian conditional probability images are the probabilistic prediction based on the trends of past 13 years (1988–2001). The Markovian conditional probability of being built-up ranges up to 0.59, which is highest among all other LULC classes. The probability values range up to 0.44 for agricultural land, up to 0.14 for dense vegetation, up to 0.46 for sparse vegetation, up to 0.22 for fallow land, up to 0.47 for water bodies, and up to 0.39 for sand. Now, by aggregating all the produced Markovian conditional probability images, a single LULC map for future prediction is generated. A stochastic choice decision model is used to perform this prediction. It creates a stochastic LULC map by assessing and combining all the conditional probabilities in which each LULC class can be present at each pixel location against a rectilinear random allocation of probabilities (Ahmed and Ahmed 2012).

### CA-MC model-based prediction

To predict an LULC map for the year 2015, two different LULC maps of the years 1988 and 2001 were used to create

**Table 8** Transition probabilities of change among LULC for Markov chain (1988–2001) for 2015 in MLP modeling

LULC class	Agricultural land	Dense vegetation	Sparse vegetation	Fallow land	Built up	Water bodies	Sand
Agricultural land	0.1835	0.0751	0.3256	0.1145	0.2945	0.0065	0.0003
Dense vegetation	0.3104	0.1650	0.4445	0.0405	0.0308	0.0087	0.0001
Sparse vegetation	0.4041	0.1020	0.3702	0.0916	0.0255	0.0065	0.0001
Fallow land	0.4127	0.0825	0.3328	0.1433	0.0082	0.0145	0.0060
Built up	0.0289	0.0226	0.0451	0.0315	0.8546	0.0117	0.0056
Water bodies	0.0663	0.0440	0.1433	0.0725	0.0178	0.5494	0.1067
Sand	0.0523	0.0009	0.0547	0.1977	0.0009	0.2294	0.4641

**Table 9** Transition probabilities of change among LULC for Markov chain (2001–2015) for 2030 in MLP modeling

LULC class	Agricultural land	Dense vegetation	Sparse vegetation	Fallow land	Built up	Water bodies	Sand
Agricultural land	0.1652	0.0695	0.2967	0.1383	0.3285	0.0011	0.0007
Dense vegetation	0.2892	0.1602	0.4312	0.0683	0.0475	0.0034	0.0002
Sparse vegetation	0.3865	0.1051	0.3823	0.0927	0.0315	0.0017	0.0002
Fallow land	0.4311	0.0465	0.3422	0.1563	0.0114	0.0057	0.0068
Built up	0.0104	0.0118	0.0642	0.0281	0.8802	0.0038	0.0015
Water bodies	0.0694	0.0312	0.1264	0.0779	0.0216	0.5603	0.1132
Sand	0.0454	0.0001	0.0009	0.1708	0.0052	0.2129	0.5647

the transition probability matrix. The suitability images are created by setting transition rules from one LULC class to another class. In the present study, physical factors are only regarded as drivers of changes in LULC.

The physical proximity to an existing LULC class is assumed to be a driver of change into a specific LULC class in the future. The rules and suitability maps were prepared for each LULC class. The fundamental supposition for producing suitability images is the pixel nearer to an existing LULC class that has the higher suitability. In suitability images, the values ranged from 0 to 255, with 0 being unsuitable and 255 being highly suitable. Therefore, for this fundamental supposition, a simple linear distance decay function is adequate. It provides the fundamental idea of contiguity, and a fuzzy-set membership analysis procedure (Eastman 2009) is used to standardize LULC maps to the same continuous suitability scale (0–255).

### MLP-MC model-based prediction

The MLPNN analysis was used to determine the weights of transitions for the period of 1988 to 2001 that will be included in the transition probability matrix using MC analysis for future prediction. The transition probability matrix is the cross-tabulation of two LULC maps of different years (1988 and 2001) and is shown in Table 8. In the transition probability matrix, rows and columns stand for

the earlier and later date images. The MC analysis is a random process and very helpful in determining the measure, behaviors, and frequencies of LULCC in a region by analyzing LULC maps of two dates. Based on all transition potential maps created for various LULC transitions, the MLPNN was applied with an accuracy of 87.56% with 10,000 iterations.

Further, Table 8 exhibits that the probability of change of agricultural land into built up area in the future date in 2015 from 1988 to 2001 is 29.45%, while the probability of changing of agricultural land into agricultural land in the future is only 18.35%. The probabilities of changing of agricultural land into built up area raised up to 32.85 and 33.55% in 2030 and 2050, respectively. Alternatively, the probabilities of changing of agricultural land into agricultural land in future dates reduced continuously to 16.52 and 15.85% in 2030 and 2050, respectively. On the other hand, the probabilities of changing of agricultural land into built up area increased remarkably from 29.45 to 32.85 and 33.55% in 2030 and 2050, respectively. Markov transition probability matrices of changing among LULC classes for years 2030 and 2050 are given in Tables 9 and 10. It is notified through the quantitative and qualitative analyses of LULC maps of different years that there is rapid expansion of built up area in Varanasi district of Uttar Pradesh, India, which needs to be analyzed and modeled further.

**Table 10** Transition probabilities of change among LULC for Markov chain (2001–2015) for 2050 in MLP modeling

LULC class	Agricultural land	Dense vegetation	Sparse vegetation	Fallow land	Built up	Water bodies	Sand
Agricultural land	0.1585	0.0759	0.2871	0.1421	0.3355	0.0007	0.0002
Dense vegetation	0.2852	0.1682	0.4529	0.0528	0.0371	0.0037	0.0001
Sparse vegetation	0.3952	0.1102	0.3916	0.0806	0.0205	0.0017	0.0002
Fallow land	0.4356	0.0309	0.3353	0.1494	0.0372	0.0061	0.0055
Built up	0.0248	0.0131	0.0504	0.0115	0.8953	0.0019	0.0030
Water bodies	0.0549	0.0292	0.1197	0.0595	0.0379	0.5795	0.1193
Sand	0.0496	0.0091	0.0062	0.1473	0.0108	0.2005	0.5765



**Table 11** Kappa index statistics for the ST-MC, CA-MC, and MLP-MC prediction results

Agreement	ST-MC	CA-MC	MLP-MC
$K_{no}$	0.7835	0.8581	0.8860
$K_{location}$	0.7977	0.8684	0.8948
$K_{location\ strata}$	0.7977	0.8684	0.8948
$K_{standard}$	0.7684	0.8302	0.8681

**Validation and selection of model**

In the present study, three hybrid models (ST-MC, CA-MC, and MLP-MC) are used to predict future LULC scenarios. Three hybrid models were first compared to facilitate a valid prediction for future LULC scenario. The values of kappa index statistics for all three models are given in Table 11. It is clear from the table that  $K_{no}$ ,  $K_{location}$ ,  $K_{location\ strata}$ , and  $K_{standard}$  values for the MLP-MC-based, predicted LULC map of 2015 are higher in comparison to those of CA-MC and ST-MC models. It is showing a strong-to-perfect agreement between predicted and observed LULC maps because all values of kappa index statistics are greater than 0.80. The MLP-MC hybrid model provided the best results in comparison to other modeling methods for the study area. Finally, the future LULC scenarios were predicted quantitatively and

spatially for year 2030 and 2050 by the better result-providing MLP-MC model.

**Prediction and analysis of future LULC scenarios for 2030 and 2050 using the MLP-MC model**

The LULC maps of 2001 and 2015 were used to predict the future LULC scenarios for years 2030 and 2050 using the MLP-MC model. Here, the method followed is the same as stated in the MLP-MC modeling section of this paper. The transition potential maps and transition probability matrices were produced using LULC maps of 2001 and 2015. By utilizing the LULC of 2015 as the base map, the transition potential maps, and the transition probability matrices of period 2001–2015, the future LULC scenarios were predicted for 2030 and 2050 as shown in Fig. 9a, b. The resultant statistics of the area for various LULC classes are represented in Table 12. The MLP-MC-based prediction results for 2030 showed that there will be a slight decrease in agricultural land (from 59.35% in 2015 to 58.32% in 2030), dense vegetation (from 4.30% in 2015 to 2.87% in 2030), sparse vegetation (from 13.36% in 2015 to 10.56% in 2030), and fallow land (from 12.56% in 2015 to 12.12% in 2030) while an increase in built up area (from 8.06% in 2015 to 14.07% in 2030).

Nevertheless, the prediction results for 2050 showed that it would experience the decrease in agricultural land (from

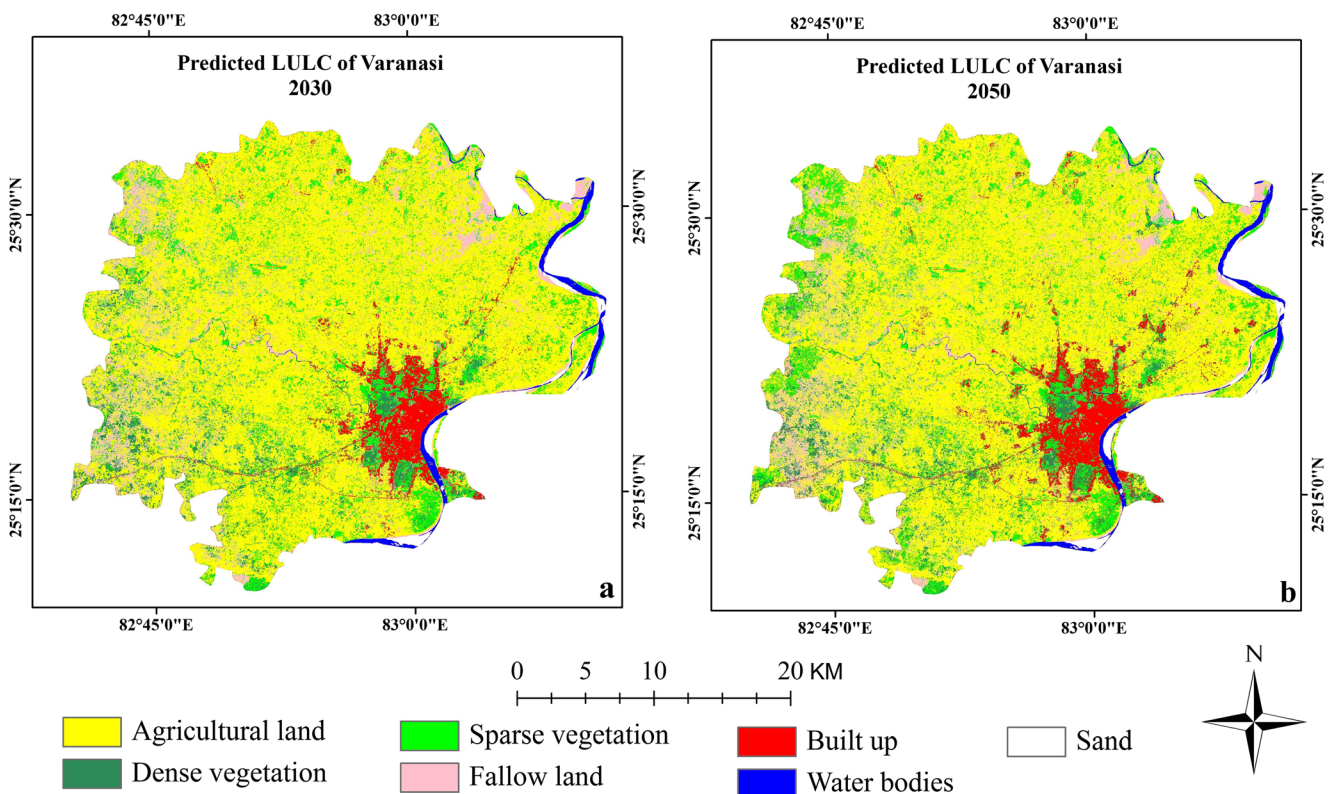


**Fig. 9** Predicted LULC maps of years 2030 and 2050

**Table 12** Area distribution of LULC for predicted years 2030 and 2050

LULC classes	Predicted 2030		Predicted 2050	
	Area (km <sup>2</sup> )	Area (%)	Area (km <sup>2</sup> )	Area (%)
Agricultural land	893.93	58.32	859.86	56.09
Dense vegetation	43.97	2.87	35.97	2.35
Sparse vegetation	161.83	10.56	132.83	8.67
Fallow land	185.86	12.12	205.86	13.43
Built up	215.68	14.07	269.68	17.59
Water bodies	20.76	1.35	18.76	1.22
Sand	10.89	0.71	9.96	0.65
Total area	1532.91	100.00	1532.91	100.00

59.35% in 2015 to 56.09% in 2050), dense vegetation (from 4.30% in 2015 to 2.35% in 2050), and sparse vegetation (from 13.36% in 2015 to 8.67% in 2050) while an increase in fallow land (from 12.56% in 2015 to 13.43% in 2050) and built up area (from 8.06% in 2015 to 17.59% in 2050). The overall loss of agricultural land and sparse vegetation occurred because of the rapid spreading of built up area while slight changes were shown by other LULC classes during 1988–2050. These results propose a worrisome change for the future scenario of the landscape of Varanasi district of Uttar Pradesh, India. Therefore, it deserves attention regarding sustainable management and development of the landscape.

## Conclusions

In this study, a combined approach of satellite remote sensing images, GIS, and prediction models was explored to understand the spatio-temporal dynamics of LULC and future scenario in Varanasi district of Uttar Pradesh, India. For this purpose, LULC patterns were examined by using Landsat TM/ETM+/OLI images of respective years 1988, 2001, and 2015. After that, the future scenario of LULC was performed proficiently using ST-MC, CA-MC, and MLP-MC hybrid models in the study area. The validation of prediction models was assessed for 2015 using kappa index statistics. Based on validation results, the MLP-MC model pointed out a descriptive capability of future prediction and was found most appropriate in comparison to ST-MC and CA-MC models.

The prediction model provides not only the description of changes quantitatively and spatially in the past but also the trend and amount of future changes. The prediction results for 2030 showed an increase of 92.20 km<sup>2</sup> in built-up area whereas a slight decrease of 15.90 km<sup>2</sup> in the agricultural land between 2015 and 2030. Furthermore, the prediction results for 2050 showed an increase of 146.20 km<sup>2</sup> in built up area whereas a decrease of 49.97 km<sup>2</sup> in agricultural land between 2015 and 2050. The analysis of LULCC between 1988 and

2050 demonstrated that there is a vast increase in built up area while a considerable reduction in agricultural land, dense vegetation, and sparse vegetation.

In this study, multiple simulation models were used to realize the future LULC prediction more accurately. Comparison of three different models enabled the recognition of prediction results using the better-performing model for the study area. However, the accuracy of prediction results is strongly related to many factors. Firstly, the accuracy of LULC maps and the prediction results is negatively affected by the moderate resolution of multi-temporal Landsat images. Second, it is assumed to have uniform transition probability in the Markov chain model. It is still not easy to include the unpredictable influence of other variables, like government policy or socioeconomic aspects. So, to achieve improved results, image quality should be increased, and new prediction models should be developed by incorporating more socioeconomic and physical variables. Moreover, this kind of study exhibited a high prospective to contribute towards the sustainable development and management of an area at the local as well as global level around the world.

**Acknowledgements** The authors wish to acknowledge the United States Geological Survey (USGS) for the free access to Landsat data used in the present study. The authors are also grateful to the anonymous reviewers for their valuable comments which helped in improving the manuscript.

## References

- Adhikari S, Southworth J (2012) Simulating forest cover changes of Bannerghatta National Park based on a CA-Markov model: a remote sensing approach. *Remote Sens* 4:3215–3243
- Ahmed B, Ahmed R (2012) Modeling urban land cover growth dynamics using multi-temporal satellite images: a case study of Dhaka, Bangladesh. *ISPRS Int J Geo-Inf* 1:3–31
- Al-sharif AA, Pradhan B (2014a) Urban sprawl analysis of Tripoli metropolitan city (Libya) using remote sensing data and multivariate logistic regression model. *J Indian Soc Remote Sens* 42(1):149–163
- Al-sharif AA, Pradhan B (2014b) Monitoring and predicting land use change in Tripoli metropolitan city using an integrated Markov chain and cellular automata models in GIS. *Arab J Geosci* 7:4291–4301
- Araya YH, Cabral P (2010) Analysis and modeling of urban land cover change in Setúbal and Sesimbra, Portugal. *Remote Sens* 2(6):1549–1563
- Arsanjani JJ, Kainz W, Mousivand AJ (2011) Tracking dynamic land-use change using spatially explicit Markov chain based on cellular automata: the case of Tehran. *Int J Image Data Fusion* 2:329–345
- Arsanjani JJ, Helbich M, Kainz W, Boloorani AD (2013) Integration of logistic regression, Markov chain and cellular automata models to simulate urban expansion. *Int J Appl Earth Obs Geoinf* 21:265–275
- Atkinson PM, Tatnall ARL (1997) Introduction neural networks in remote sensing. *Int J Remote Sens* 18(4):699–709
- Barredo JI, Kasanko M, McCormick N, Lavalle C (2003) Modelling dynamic spatial processes: simulation of urban future scenarios through cellular automata. *Landsc Urban Plan* 64:145–160
- Basharin GP, Langville AN, Naumov VA (2004) The life and work of A.A. Markov. *Linear Algebra Appl* 386:3–26

- Bhatta B (2010) Analysis of urban growth and sprawl from remote sensing data. Springer-Verlag, Heidelberg
- Bonan GB (2008) Ecological climatology—concepts and applications, 2nd edn. Cambridge University Press, Cambridge
- Bozkaya AG, Balci FB, Goksel C, Eshah H (2015) Forecasting land-cover growth using remotely sensed data: a case study of the Igneada protection area in Turkey. *Environ Monit Assess* 187:59
- Brown DG, Pijanowski BC, Duh JD (2000) Modelling the relationships between land use and land cover on private lands in the Upper Midwest, USA. *J Environ Manag* 59:247–263
- Carlson TN, Azofeifa SGA (1999) Satellite remote sensing of land use changes in and around San José, Costa Rica. *Remote Sens Environ* 70:247–256
- Clarke KC, Hoppen S (1997) A self-modifying cellular automaton model of historical urbanization in the San Francisco Bay area. *Environ Plann B Plann Des* 24:247–261
- Congalton RG, Green K (1999) Assessing the accuracy of remotely sensed data: principles and practices. CRC/Lewis, Boca Raton
- Dadhich PN, Hanaoka S (2011) Spatio-temporal urban growth modeling of Jaipur, India. *J Urban Technol* 18:45–65
- Dickinson RE (1995) Land processes in climate models. *Remote Sens Environ* 51:27–38
- Dwivedi RS, Sreenivas K, Ramana KV (2005) Land-use/land-cover change analysis in part of Ethiopia using Landsat Thematic Mapper data. *Int J Remote Sens* 26(7):1285–1287
- Eastman JR (2006) IDRISI Andes tutorial. Clark Labs, Worcester
- Eastman JR (2009) IDRISI Taiga guide to GIS and image processing; manual version 16.02. Clark Labs, Worcester
- Eastman JR (2012) IDRISI Selva Tutorial. Clark University, Worcester
- Eastman JR, Jiang H, Toledano J (1998) Multi-criteria and multi-objective decision making for land allocation using GIS. In: Beinat E, Nijkamp P (eds) *Multicriteria analysis for land use management*. Springer, Dordrecht, pp 227–251
- Fathizad H, Rostami N, Faramarzi M (2015) Detection and prediction of land cover changes using Markov chain model in semi-arid rangeland in western Iran. *Environ Monit Assess* 187:629
- Fortin MJ, Boots B, Csillag F, Remmel TK (2003) On the role of spatial stochastic models in understanding landscape indices in ecology. *Oikos* 102:203–212
- Giriraj A, Irfan-Ullah M, Murthy MSR, Beierkuhnlein C (2008) Modelling spatial and temporal forest cover change patterns (1973–2020): a case study from South Western Ghats (India). *Sensors* 8:6132–6153
- Guan D, Li H, Inohae T, Su W, Nagaie T, Hokao K (2011) Modeling urban land use change by the integration of cellular automaton and Markov model. *Ecol Model* 222:3761–3772
- Hu X, Weng Q (2009) Estimating impervious surfaces from medium spatial resolution imagery using the self-organizing map and multi-layer perceptron neural networks. *Remote Sens Environ* 113:2089–2102
- Hua L, Tang L, Cui S, Yin K (2014) Simulating urban growth using the SLEUTH model in a coastal peri-urban district in China. *Sustainability* 6:3899–3914
- Jantz CA, Goetz SJ, Shelley MK (2003) Using the SLEUTH urban growth model to simulate the impacts of future policy scenarios on urban land use in the Baltimore–Washington metropolitan area. *Environ Plann B Plann Des* 30:251–271
- Ji CY (2000) Land-use classification of remotely sensed data using Kohonen self organizing feature map neural networks. *Photogramm Eng Remote Sens* 66:1451–1460
- Kamusoko C, Aniya M, Adi B, Manjoro M (2009) Rural sustainability under threat in Zimbabwe-simulation of future land use/cover changes in the Bindura district based on the Markov-cellular automata model. *Appl Geogr* 29:435–447
- Kilic S (2006) Environmental monitoring of land use and land cover changes in a Mediterranean region of Turkey. *Environ Monit Assess* 114(1–3):157–168
- Kumar R, Nandy S, Agarwal R, Kushwaha SPS (2014) Forest cover dynamics analysis and prediction modeling using logistic regression model. *Ecol Indic* 45:444–455
- Lambin EF, Turner BL, Geist HJ, Agbola SB, Angelsen A, Bruce JW, Coomes OT, Dirzo R, Fischer G, Folke C (2001) The causes of land-use and land-cover change: moving beyond the myths. *Glob Environ Chang* 11(4):261–269
- Maithani S (2015) Neural networks-based simulation of land cover scenarios in Doon Valley, India. *Geocarto Int* 30:163–185
- Mas JF, Flores JJ (2008) The application of artificial neural networks to the analysis of remotely sensed data. *Int J Remote Sens* 29:617–663
- Mas JF, Kolb M, Paegelow M, Olmedo MTC, Houet T (2014) Inductive pattern-based land use/cover change models: a comparison of four software packages. *Environ Model Softw* 51:94–111
- Mas JF, Velazquez A, Gallegos JRD, Saucedo RM, Alcantare C, Bocco G, Castro R, Fernandez T, Vega AP (2004) Assessing land use/cover changes: a nationwide multi date spatial database for Mexico. *Int J Appl Earth Obs Geoinf* 5:249–261
- Miller AB, Bryant ES, Birnie RW (1998) An analysis of land cover changes in the northern forest of New England using multi-temporal LANDSAT MSS data. *Int J Remote Sens* 19(2):245–265
- Mishra VN, Prasad R, Kumar P, Gupta DK, Srivastava PK (2017) Dual-polarimetric C-band SAR data for land use/land cover classification by incorporating textural information. *Environ Earth Sci* 76(1):26
- Mishra VN, Rai PK (2016) A remote sensing aided multi-layer perceptron-Markov chain analysis for land use and land cover change prediction in Patna district (Bihar), India. *Arab J Geosci* 9(4):1–18
- Mishra VN, Rai PK, Mohan K (2014) Prediction of land use changes based on land change modeler (LCM) using remote sensing: a case study of Muzaffarpur (Bihar), India. *J Geogr Inst Jovan Cvijic* 64:111–127
- Mitsova D, Shuster W, Wang X (2011) A cellular automata model of land cover change to integrate urban growth with open space conservation. *Landsc Urban Plan* 99(2):141–153
- Moghadam HS, Helbich M (2013) Spatiotemporal urbanization processes in the megacity of Mumbai, India: a Markov chains-cellular automata urban growth model. *Appl Geogr* 40:140–149
- Mozumder C, Tripathi NK (2014) Geospatial scenario based modelling of urban and agricultural intrusions in Ramsar wetland Deepor Beel in Northeast India using a multi-layer perceptron neural network. *Int J Appl Earth Observ Geoinf* 32:92–104
- Mozumder C, Tripathi NK, Losiri C (2016) Comparing three transition potential models: a case study of built-up transitions in North-East India. *Comput Environ Urban Syst* 59:38–49
- Muller R, Middleton J (1994) A Markov model of land-use change dynamics in the Niagara region, Ontario, Canada. *Landsc Ecol* 9:151–157
- Olmedo MTC, Paegelow M, Mas JF (2013) Interest in intermediate soft-classified maps in land change model validation: suitability *versus* transition potential. *Int J Geogr Inf Sci* 27:2343–2361
- Paudel S, Yuan F (2012) Assessing landscape changes and dynamics using patch analysis and GIS modeling. *Int J Appl Earth Observ Geoinf* 16:66–76
- Pijanowski BC, Pithadia S, Shellito BA, Alexandridis K (2005) Calibrating a neural network based urban change model for two metropolitan areas of the Upper Midwest of the United States. *Int J Geogr Inf Sci* 19:197–215
- Pontius RG (2000) Quantification error versus location error in comparison of categorical maps. *Photogramm Eng Remote Sens* 66:1011–1016
- Prenzel B (2004) Remote sensing-based quantification of land-cover and land-use change for planning. *Prog Plan* 61:281–299

- Seto KC, Woodcock CE, Song C, Huang X, Lu J, Kaufmann RK (2002) Monitoring land use change in the Pearl River Delta using Landsat TM. *Int J Remote Sens* 23(10):1985–2004
- Tang J, Wang L, Yao Z (2007) Spatio-temporal urban landscape change analysis using the Markov chain model and a modified genetic algorithm. *Int J Remote Sens* 28(15):3255–3271
- Thapa RB, Murayama Y (2012) Scenario based urban growth allocation in Kathmandu Valley, Nepal. *Landsc Urban Plan* 105:140–148
- Thies B, Meyer H, Nauss T, Bendix J (2014) Projecting land use and land-cover changes in a tropical mountain forest of Southern Ecuador. *J Land Use Sci* 9(1):1–33
- Triantakoustantis D, Mountrakis G (2012) Urban growth prediction: a review of computational models and human perceptions. *J Geogr Inf Syst* 4:555–587
- Vapnik VN (1999) An overview of statistical learning theory. *IEEE Trans Neural Netw* 10(5):988–999
- Veldkamp A, Fresco LO (1996) CLUE: a conceptual model to study the conversion of land use and its effects. *Ecol Model* 85:253–270
- Verburg PH, de Nijs TCM, RitsemavanEck J, Visser H, de Jong K (2004) Method to analyse neighbourhood characteristics of land use patterns. *Comput Environ Urban Syst* 28:667–690
- Wang SQ, Zheng XQ, Zang XB (2012) Accuracy assessments of land use change simulation based on Markov-cellular automata model. *Procedia Environ Sci* 13:1238–1245
- Weng Q (2002) Land use change analysis in the Zhujiang Delta of China using satellite remote sensing, GIS and stochastic modelling. *J Environ Manag* 64:273–284
- Zhu Z, Liu L, Chen Z, Zhang J, Verburg PH (2010) Land-use change simulation and assessment of driving factors in the loess hilly region—a case study as Pengyang County. *Environ Monit Assess* 164:133–142
- Zhu Z, Woodcock CE (2014) Continuous change detection and classification of land cover using all available Landsat data. *Remote Sens Environ* 144:152–171